Supplementary information

Pressure-induced structural transitions and metallization in two-dimensional semiconductor of $CuInP_2S_6$

Meiling Hong,[a,b] Lidong Dai,[*c] Haiying Hu,[c] Xinyu Zhang,[a,b] Xuefei Liu,[c] Ziqiang Xu,[c] Juxiang Shao[a,b]

AFFILIATIONS

[a]Key Laboratory of Computational Physics of Sichuan Province, College of Mathematics and Physics, Yibin University, Yibin 644007, China;

[b]College of Mathematics and Physics, Yibin University, Yibin 644007, China;

[c]School of Physics and Electronic Science, Guizhou Normal University, Guiyang, 550025, China

[*]Author to whom correspondence should be addressed: dailidong@gznu.edu.cn

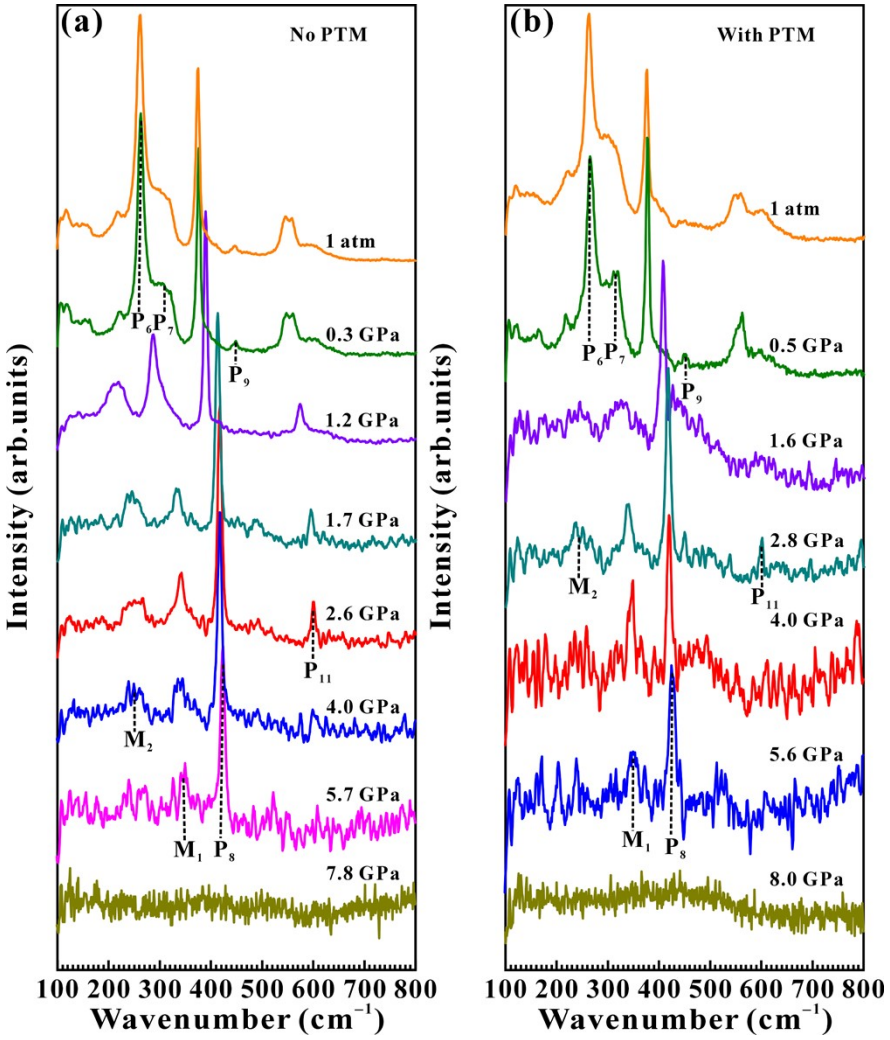

Figure S1. High-pressure Raman spectra of $CuInP_2S_6$ during the process of decompression under (a) non-hydrostatic condition and (b) hydrostatic condition, respectively. Herein, the signal of PTM denotes pressure transmitting medium.

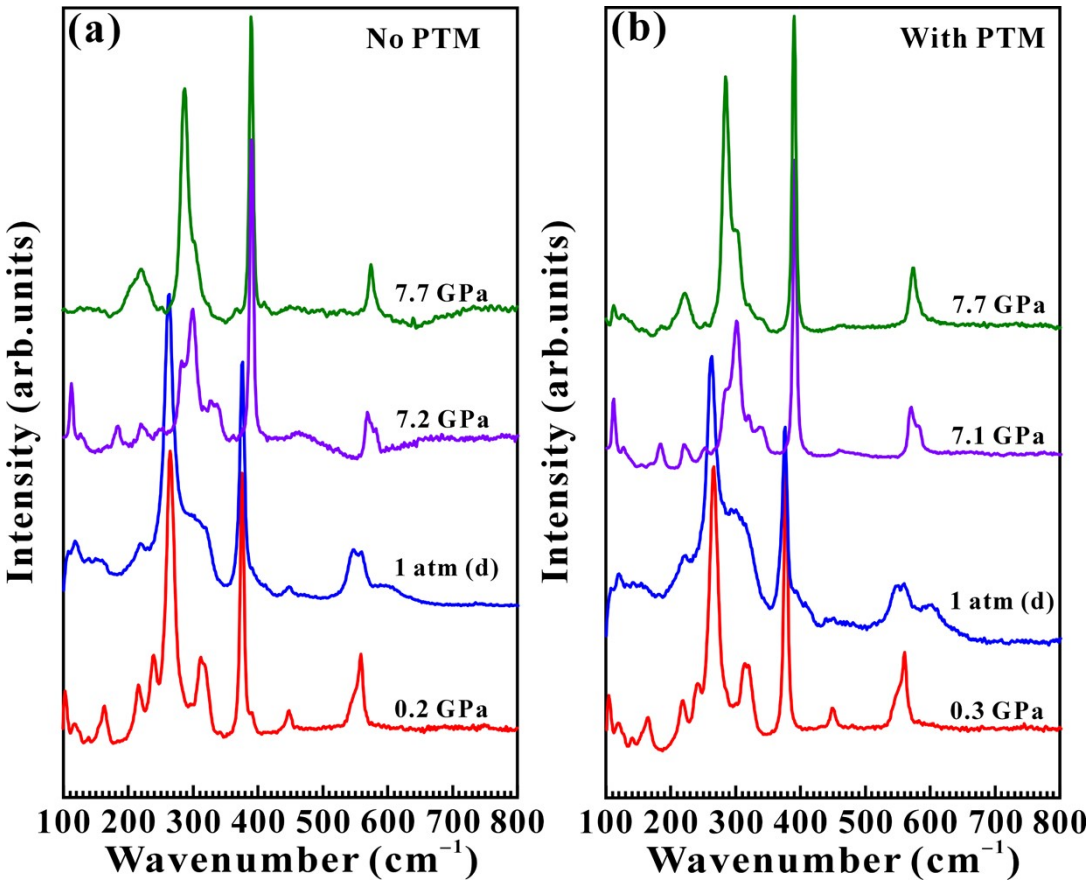

Figure S2. The comparison of Raman spectra for the pressurized and recovered samples under (a) non-hydrostatic condition and (b) hydrostatic condition, respectively. Herein, the signals of d and PTM denote decompression and pressure transmitting medium, respectively.

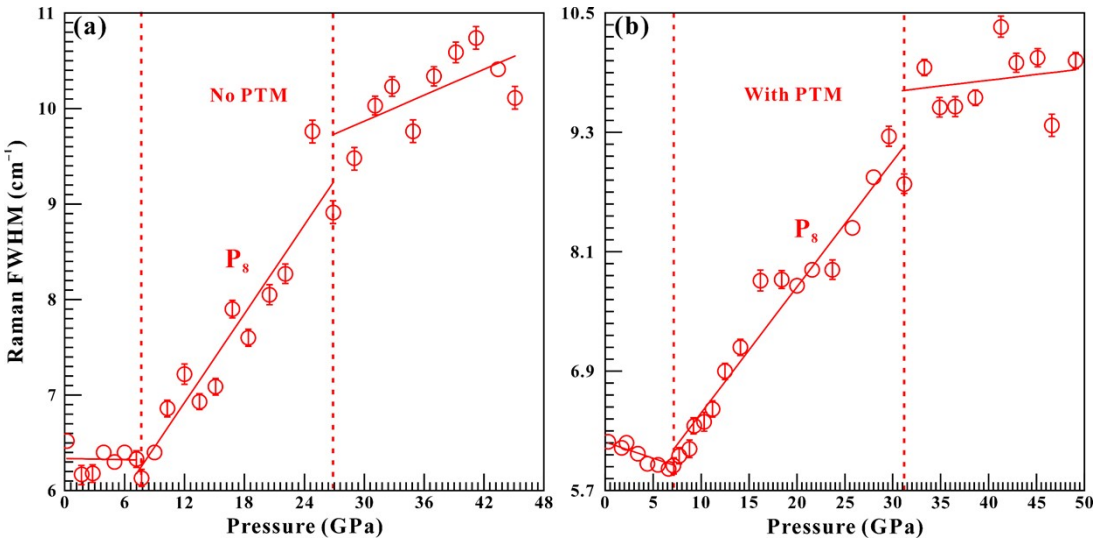

Figure S3. Pressure-dependent Raman FWHM relations for P_8 mode under (a) non-hydrostatic condition and (b) hydrostatic condition, respectively. The errors in Raman FWHMs are within the size of the symbols. Herein, the signal of PTM signifies pressure transmitting medium.

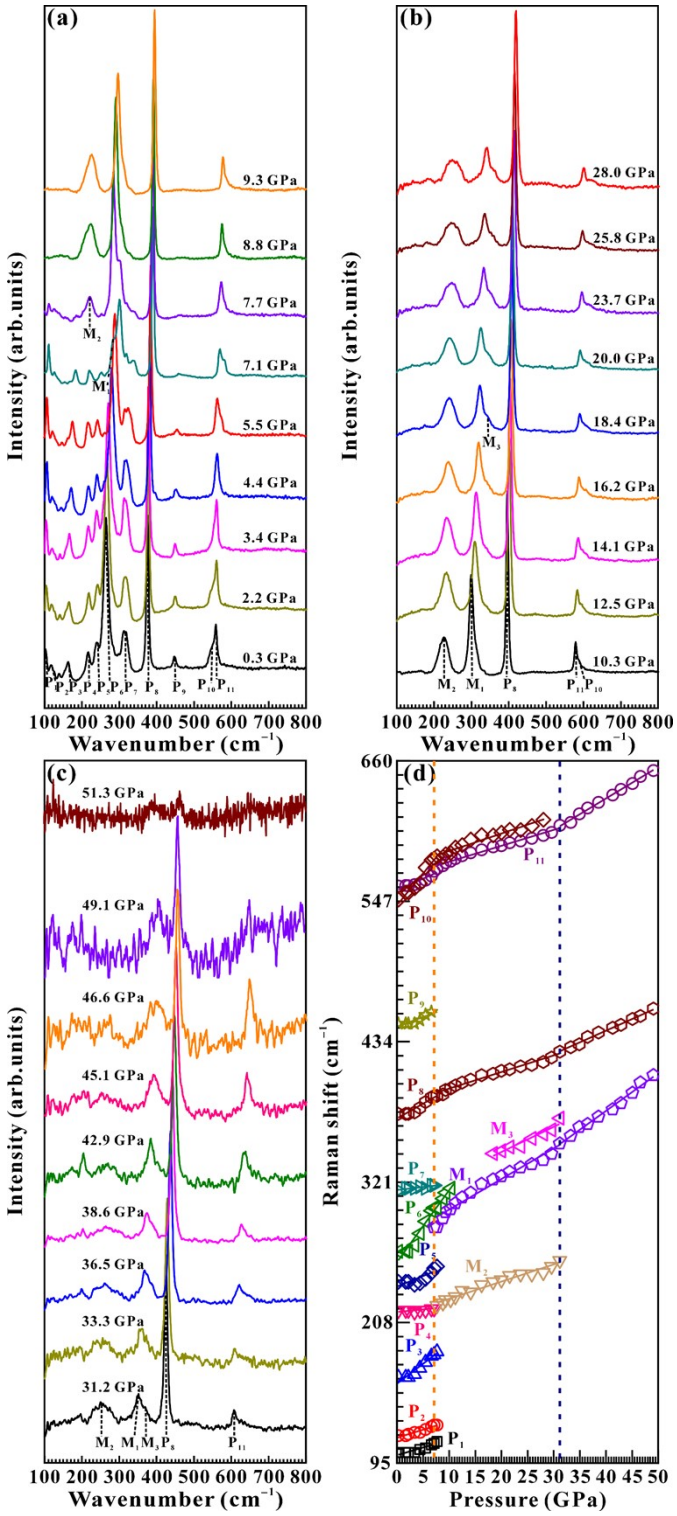

Figure S4. High-pressure Raman scattering patterns of $CuInP_2S_6$ under hydrostatic condition. (a–c) The results from 0.3 to 51.3 GPa upon compression. (d) The correspondent variation of Raman shifts as a function of pressure. The errors in Raman shifts are within the size of the symbols.

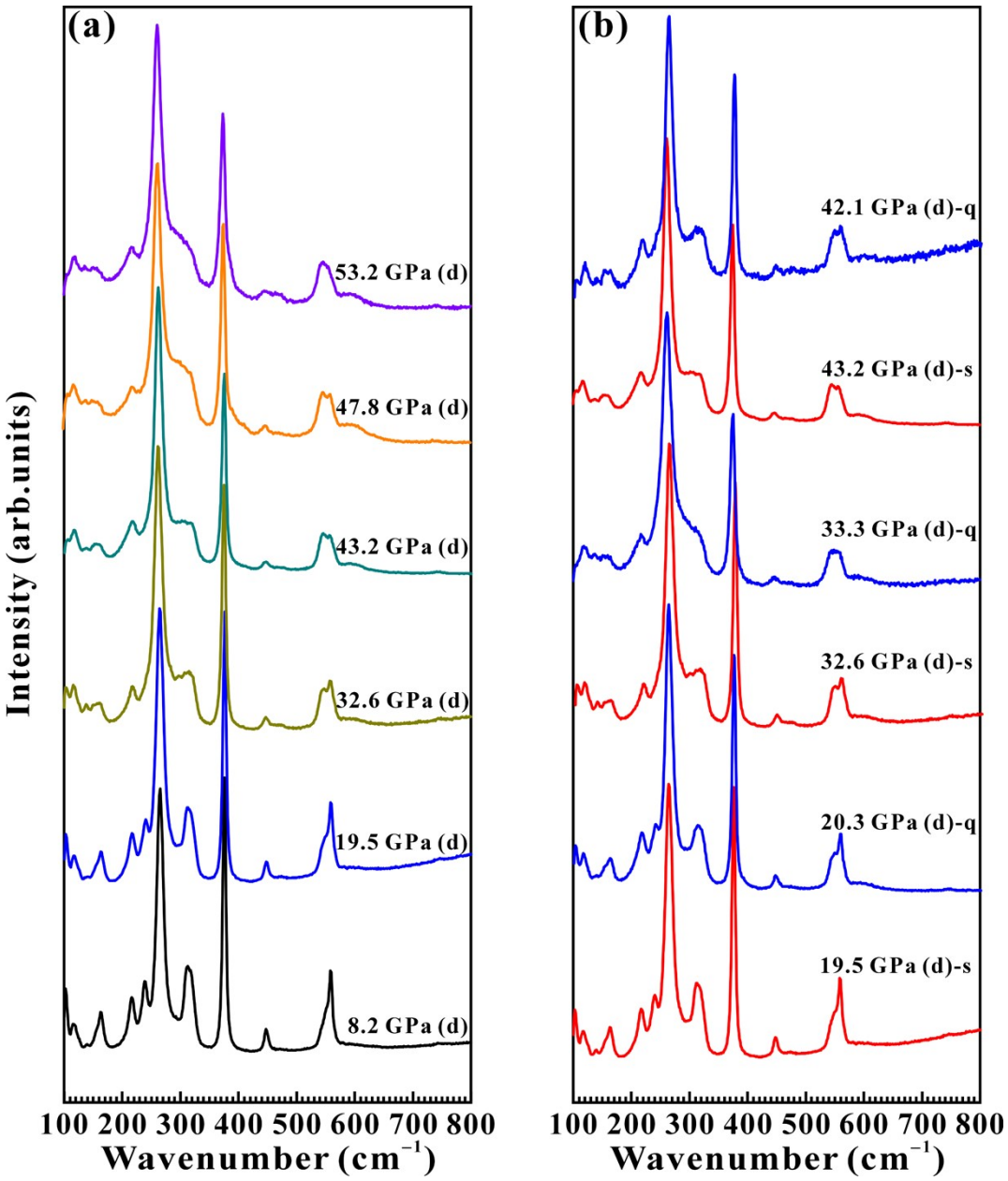

Figure S5. Raman spectra of $CuInP_2S_6$ (a) released from the different highest experimental pressures of 8.2, 19.5, 32.6, 43.2, 47.8 and 53.2 GPa at similar decompression rate of ~1 GPa/hour and (b) decompressed from the analogous pressures of ~20.0, ~33.0 and ~43.0 GPa with different decompression rates of ~1 GPa/min and ~1 GPa/hour. Herein, the signals of d, s and q stand for decompression, slower decompression rate of ~1 GPa/hour and quicker decompression rate of ~1 GPa/min, respectively.

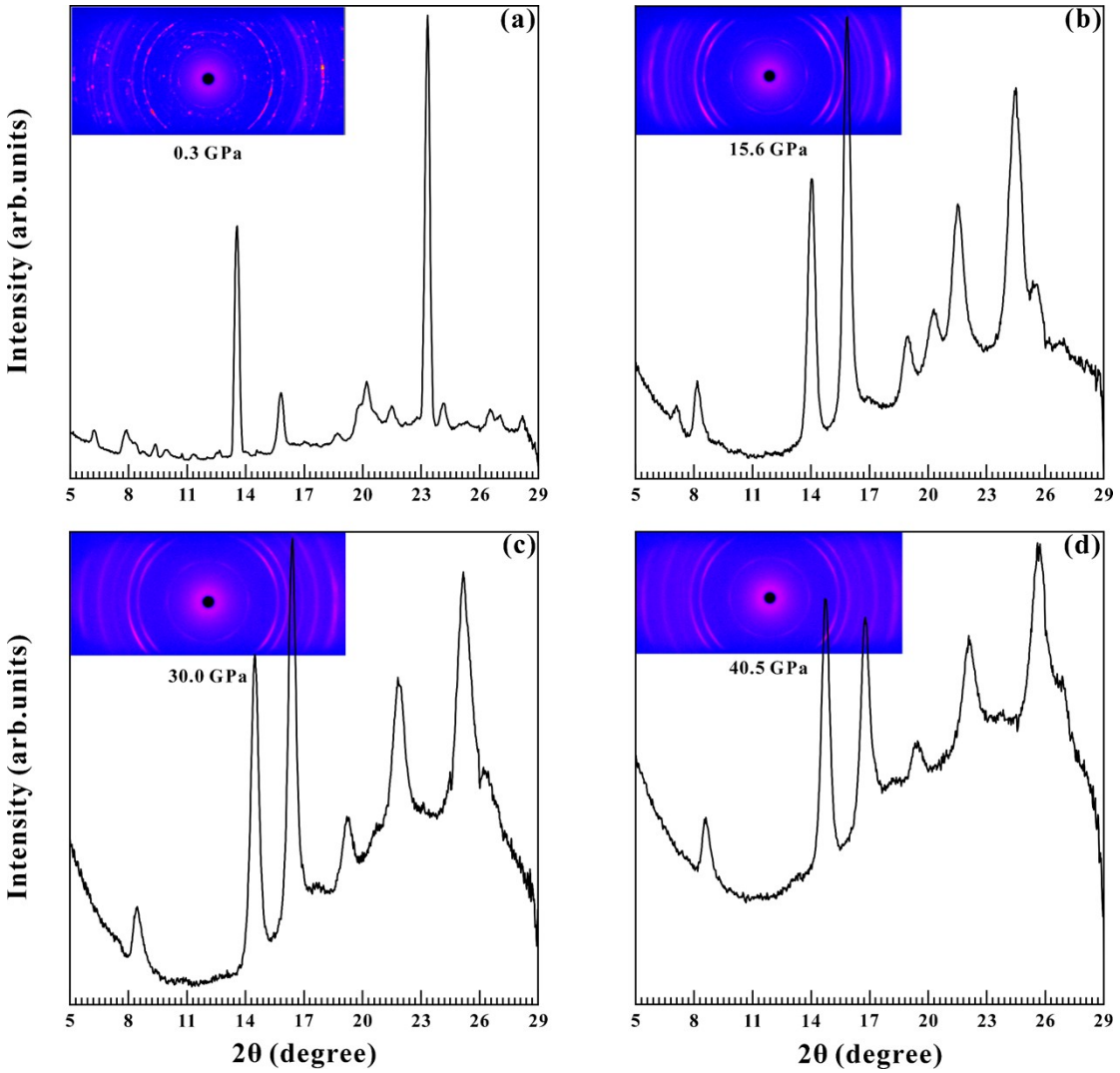

Figure S6. High-pressure micro-area XRD profiles and the correspondent 2D diffraction rings for $CuInP_2S_6$ at four representative pressures of (a) 0.3 GPa, (b) 15.6 GPa, (c) 30.0 GPa and (d) 40.5 GPa, respectively.

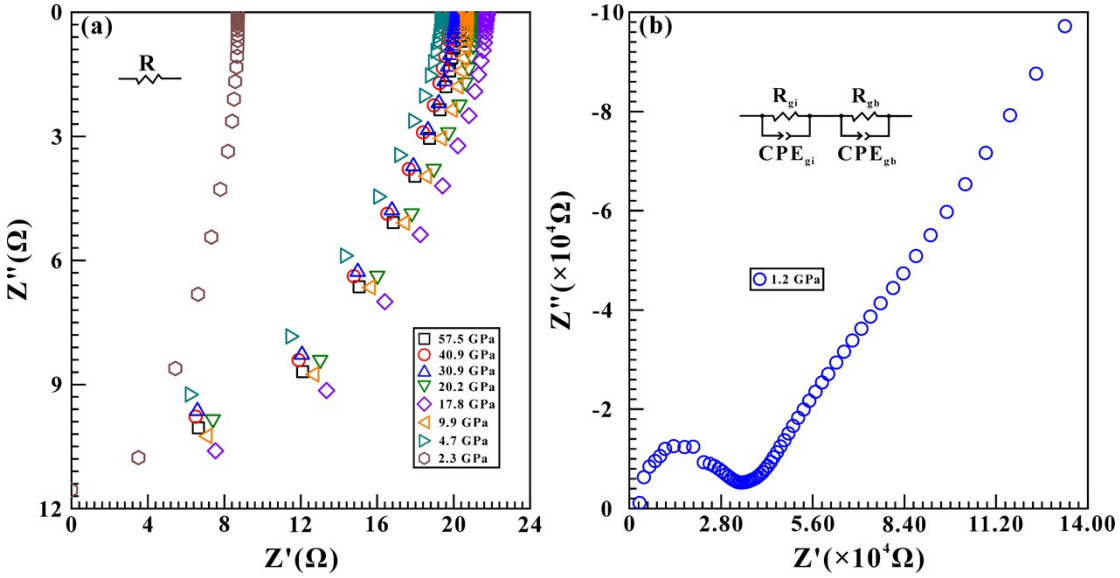

Figure S7. The selected impedance spectra of decompressed sample at (a) 57.5–2.3 GPa and (b) 1.2 GPa. Herein, the signals of Z′ and Z″ represent the real and imaginary components of the complex impedance, respectively.

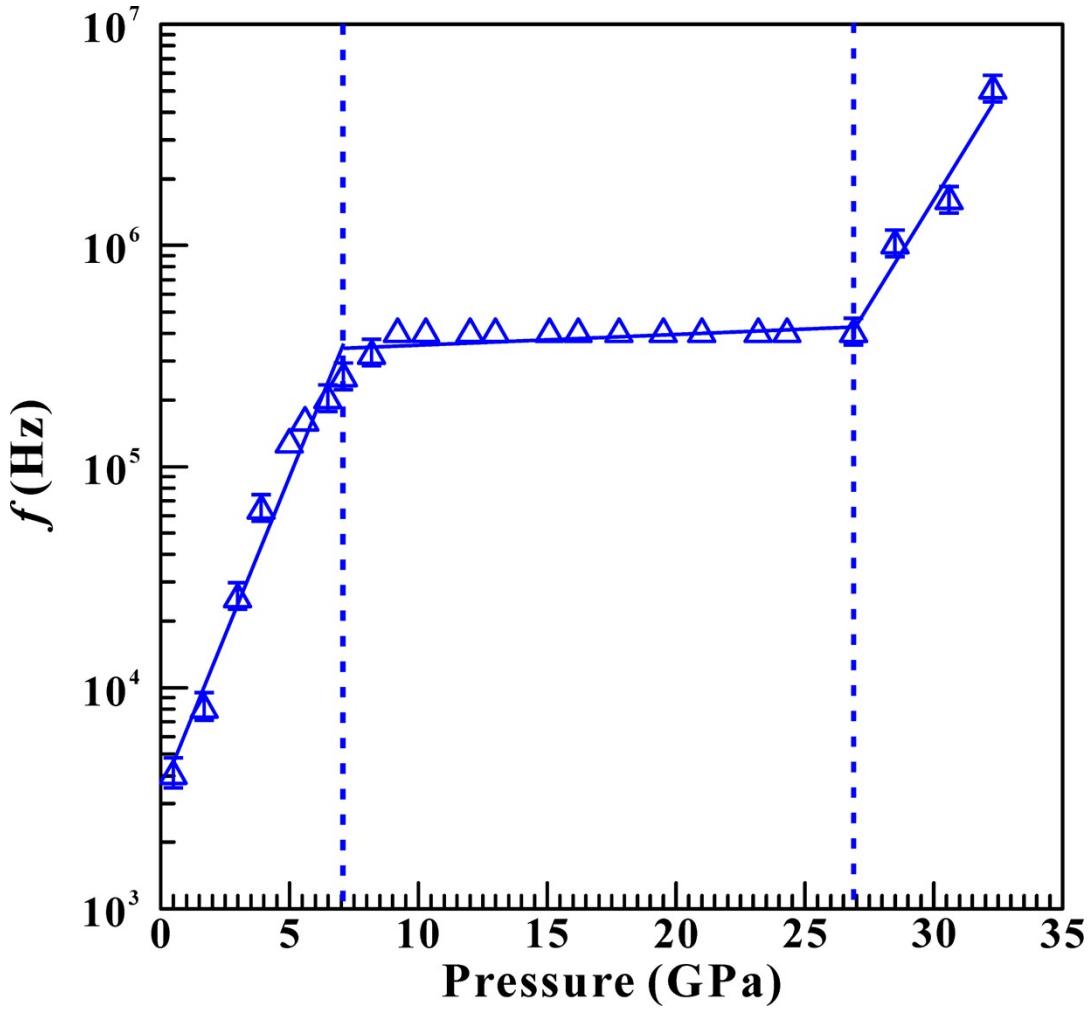

Figure S8. The evolution of relaxation frequency as a function of pressure at room temperature for $CuInP_2S_6$. Herein, the signal of *f* refers to relaxation frequency. The errors in relaxation frequencies are within the size of the symbols.

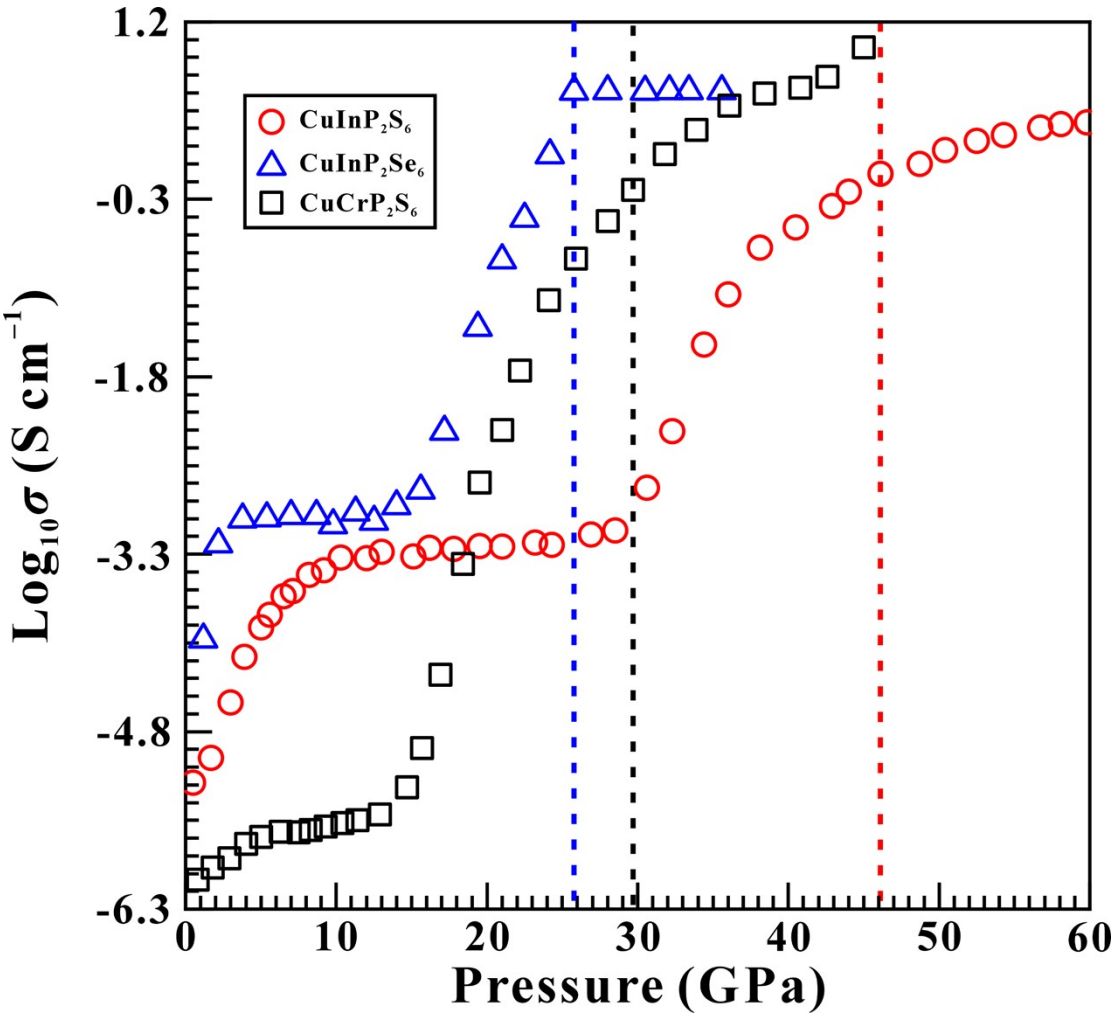

Figure S9. The comparison of the pressure-dependent logarithmic electrical conductivity relations for $CuMP_2X_6$ (M = Cr and In; X = S and Se) reported in this work and previous studies.

Table S1. Pressure-dependent Raman shift ($d\omega/dP$, cm^{-1} GPa^{-1}) for $CuInP_2S_6$ upon pressurization under different hydrostatic environments. Herein, the signals of ω (cm^{-1}) and P (GPa) represent Raman frequency and pressure, respectively.

Pressure condition	Pressure range (GPa)	ω (cm^{-1})	$d\omega/dP$ (cm^{-1} GPa^{-1})	ω (cm^{-1})	$d\omega/dP$ (cm^{-1} GPa^{-1})
Non-hydrostatic	0.2–7.2	103.5 (P_1)	1.32	118.3 (P_2)	1.16
		163.9 (P_3)	3.04	216.6 (P_4)	0.34
		239.7 (P_5)	1.27	265.2 (P_6)	5.50
		312.3 (P_7)	2.13	376.0 (P_8)	2.16
		448.6 (P_9)	1.64	549.9 (P_{10})	4.56
		559.2 (P_{11})	3.45		
	7.2–26.9	112.2 (P_1)	–	125.8 (P_2)	–
		183.5 (P_3)	–	–	
		248.2 (P_5)	–	299.1 (P_6)	5.12
		326.8 (P_7)	–	389.2 (P_8)	1.94
		–		577.5 (P_{10})	2.33
		579.8 (P_{11})	1.68	282.2 (M_1)	3.54
		219.0 (M_2)	2.43	333.9 (M_3)	2.53
	26.9–45.1	–		–	
		–		–	
		–		–	
		–		428.5 (P_8)	1.57
		–		619.3 (P_{10})	0.71
		610.5 (P_{11})	2.13	355.7 (M_1)	2.16
		267.6 (M_2)	–	370.0 (M_3)	–
Hydrostatic	0.3–7.1	103.5 (P_1)	1.15	117.1 (P_2)	1.30
		163.9 (P_3)	3.09	217.5 (P_4)	0.21
		240.8 (P_5)	1.44	265.3 (P_6)	5.91

	314.2 (P_7)	0.51	376.0 (P_8)	2.38
	448.6 (P_9)	1.59	548.4 (P_{10})	5.16
	559.2 (P_{11})	1.60		
	110.9 (P_1)	2.17	125.7 (P_2)	1.30
	182.3 (P_3)	4.00	–	
	251.8 (P_5)	2.17	300.3 (P_6)	5.44
7.1–31.2	318.4 (P_7)	–	390.3 (P_8)	1.36
	–		581.4 (P_{10})	1.44
	571.0 (P_{11})	1.32	284.6 (M_1)	2.53
	221.5 (M_2)	1.42	343.9 (M_3)	2.02
	–		–	
	–		–	
	–		–	
31.2–49.1	–		426.1 (P_8)	1.88
	–		–	
	608.1 (P_{11})	2.52	352.1 (M_1)	3.04
	257.9 (M_2)	–	372.5 (M_3)	–

Table S2. Pressure-dependent Raman full width at half maximum (FWHM) (dF/dP, cm^{-1} GPa^{-1}) for $CuInP_2S_6$ upon pressurization under different hydrostatic environments. Herein, the signals of ω (cm^{-1}), F (cm^{-1}) and P (GPa) stand for Raman frequency, Raman FWHM and pressure, respectively.

Pressure condition	Pressure range (GPa)	ω (cm^{-1})	F (cm^{-1})	dF/dP (cm^{-1} GPa^{-1})
Non-hydrostatic	0.2–7.2	376.0 (P_8)	6.12	–0.0020
	7.2–26.9	389.2 (P_8)	5.93	0.15
	26.9–45.1	428.5 (P_8)	8.51	0.045
Hydrostatic	0.3–7.1	376.0 (P_8)	6.19	–0.043
	7.1–31.2	390.3 (P_8)	5.95	0.13
	31.2–49.1	426.1 (P_8)	8.78	0.012

Table S3. The comparison on the phase transition pressure and reversibility of $CuInP_2S_6$ (CIPS) reported in this work and previous studies. Here, the signals of P_{tr}, P_m, PTM and MEW represent phase transition pressure, maximum experimental pressure, pressure transmitting medium and the mixture of methanol, ethanol and water (16:3:1 volume ratio), respectively.

Samples	P_{tr} (GPa)	P_m (GPa)	PTM	Reversibility	References
CIPS powder	7.2 26.9 47.8	47.8	No	Irreversible	This work
	7.7 31.2 51.3	51.3	Helium		
CIPS crystals	~4.0	17.5	CsI	Reversible	[8]
CIPS single-crystal flakes	5.4	14.9	Neon	Reversible	[9]
CIPS crystals	3.7	25.1	–	–	[10]
CIPS single crystals	5.0 5.0–12.0 12.0–17.0	20.0	MEW	Reversible	[11]
CIPS single crystals	~4.0	9.56	Silicone oil	–	[12]

Table S4. The pressure dependence of activation energy (dH/dP, meV GPa^{-1}) for $CuInP_2S_6$ within three distinct pressure ranges of 0.5–7.1 GPa, 7.1–26.9 GPa and 26.9–32.3 GPa, respectively. Wherein, the signals of H (meV) and P (GPa) refer to activation energy and pressure, respectively.

Pressure range (GPa)	dH/dP (meV GPa^{-1})	Error (%)
0.5–7.1	–17.56	0.28
7.1–26.9	–0.12	0.33
26.9–32.3	–6.66	1.83

Table S5. The metallization pressure (P_m) of $CuMP_2X_6$ (M = Cr and In; X = S and Se) reported in this work and previous studies.

Samples	P_m (GPa)	References
$CuInP_2S_6$	48.7	This work
$CuInP_2Se_6$	25.8	[17]
$CuCrP_2S_6$	29.7	[16]